(Received 17 February 2025, Accepted 21 March 2025, Scheduled 28 April 2025)

Design of Polarization-Insensitive Wideband Metamaterial Radar Absorber with Enhanced Bandwidth

Muhammad A. Baqir[1, *], Abdul Qadeer[1], Olcay Altintas[2, 5], Muhammad U. Draz[1], Muharrem Karaaslan[3, 5], and Jahariah Sampe[4]

[1]*Department of Electrical and Computer Engineering, COMSATS University Islamabad, Sahiwal Campus, Pakistan*
[2]*Department of Avionics, Iskenderun Technical University, Iskenderun, Hatay 31200, Turkey*
[3]*Department of Electrical and Electronics Engineering, Iskenderun Technical University, Iskenderun, Hatay 31200, Turkey*
[4]*Institute of Microengineering and Nanoelectronics (IMEN), Universiti Kebangsaan Malaysia (UKM), Malaysia*
[5]*ISTE Center for Science and Technology Studies and Research (ISTE-CSTSR), Turkey*

ABSTRACT: Metamaterial-based absorbers offering perfect and broadband absorption are greatly desirable in radar and stealth technology systems. Further, the polarization insensitive feature makes the absorber useful for industrial applications. This study examines the design of a wideband metamaterial-based radar absorber functioning throughout the frequency range of 8 to 16 GHz. The metasurface design comprises two concentric metallic rings and a fan-shaped circular metallic disc at the middle. The rings and central disc are interconnected with surface-mounted chip resistors to enhance the absorption bandwidth. It is depicted that more than 90% absorptivity was attained from 8 to 16 GHz. A wideband absorber with angular stability and polarization insensitivity is an excellent choice for wireless communications, particularly in radar applications. Further, the measured results of the prototype corresponded well with the simulated outcomes.

1. INTRODUCTION

Metamaterials (MMs) show unique electromagnetic characteristics because of the periodic nature of subwavelength-sized unit cells. Natural materials cannot provide the unique electromagnetic properties achievable with MMs [1–7]. MMs are found in many novel applications, like lenses [8], cloaking [9–11], filters [12–14], sensors [15–17], energy harvesting [18–20], and absorbers [21–27]. The first proposal on the MM-based absorber was made by Landy et al. [28]. Subsequently, numerous absorbers in the microwave and optical domains have been developed utilizing metasurfaces composed of various resonators, including cross-resonators, square rings, split-ring resonators (SRRs), and trapezoidal arrays [21–27].

MM-based absorbers with wideband absorption find immense potential in radar and stealth applications [29, 30]. Much research has been conducted in designing absorbers for X-band frequencies, but most of them suffer from narrow bandwidth and complex design [31–33]. To meet the stringent requirements of radar and stealth applications, there is a need for a simple design of the absorbers with perfect and wideband absorption. This opens up a window of opportunity for researchers to design efficient and economical metamaterial-based absorbers with wideband absorption response.

Various techniques are used to broaden the absorptivity in the optical regime, including nanowires [34], supercells made using an in-plane arrangement of multiple resonators [35], and multilayer vertically metallic/dielectric layers [36, 37]. Although absorption spectrum of the absorber can be broadened by these techniques, these techniques suffer from complex structures and challenging fabrication processes. To achieve broadband absorption in the microwave regime, multilayered vertically stacked resonant elements are used, which makes the design complex, bulky, and costly [38–40]. Consequently, the development of an absorber characterized by broad absorption, cost-effectiveness, compact dimensions, and a straightforward fabrication technique is imperative.

The utilization of resistances in the design is an effective technique to enhance the absorption spectrum of an absorber [41–45]. This study seeks to use lumped chip resisters among the distributed elements to enhance and improve the absorption spectrum of the structure. The chip resistors used in the absorber design are low cost and easy to install which make this design an ideal choice for robust applications like radar and stealth technology. The metasurface of the design is constituted of resonators with two concentric metal rings and a fan-shaped circular metal disc in the center. The circular rings facilitate the circulation of incoming surface currents generated by electromagnetic waves, inducing resonance that subsequently enhances absorption. The fan-like structure produces a capacitive effect, while chip resistors increase ohmic loss. Consequently, the proposed structure possesses the capability to enhance absorption. More than 80% absorptivity is achieved from 8 to 17 GHz. The polarization-insensitive and angle-insensitive (ranging from 0° to 50°) features make the absorber useful for microwave applications. In the forthcoming part of the paper, Section 2 discusses the design and theory. Results and discussion are reported in Section 3. Section 4 covers the conclusion of the paper.

* Corresponding author: Muhammad Abuzar Baqir (abuzar@cuisahiwal.edu.pk).

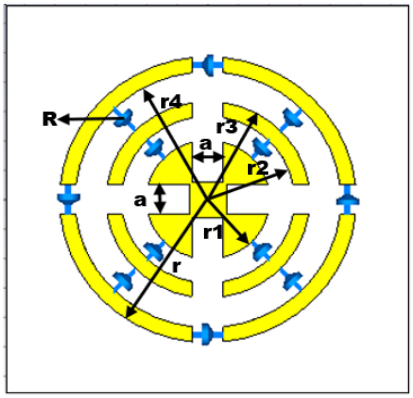

FIGURE 1. Proposed metamaterial-based absorber.

2. DESIGN AND THEORY

The design of the unit of the chip-resistors based absorber is demonstrated in Fig. 1. The unit cell consists of three layers: an upper metasurface, a central dielectric substrate, and a lower metallic layer. The thickness of the top metasurface and bottom layer is kept at 0.035 mm. The unit cell (with period 13 mm) of the proposed structure is made of a fan enclosed in the split rings. Further, this structure is an excellent choice because of its symmetry which makes it polarization-insensitive. The resistors are incorporated within the cuts of the top metasurface structure. The middle FR-4 dielectric substrate isolates the design from the ground and is 2.9 mm thick. The parametric values of the unit cell of the absorber are represented in Table 1.

TABLE 1. The parametric values used for the design of the absorber.

Parameters	Value (mm)	Parameters	Value (mm)
a	1	r_3	3.3
r_1	2	r_4	4.5
r_2	2.8	r	5
R	200 Ω		

The incoming electromagnetic waves penetrate inside the absorber structure due to resonance at top metasurface. The middle layer of the absorber keeps trapping the waves, and transmission remains blocked by the bottom layer. The wave inside the substrate transforms to the other form by energy by the Fabry-Perot effect. The absorber's unit cell was simulated using CST Microwave Studio. The simulation configuration includes periodic boundary conditions in the xy-plane and open boundary conditions along the z-axis. A plane wave is excited at the surface of the absorber.

We have determined the absorption considering the transmission and reflection coefficients in terms of S-parameters. Absorption is calculated using Eq. (1)

$$A(\omega) = 1 - |S_{11}(\omega)|^2 - |S_{21}(\omega)|^2 \quad (1)$$

$A(\omega)$ represents the absorption, whereas $|S_{21}(\omega)|^2$ and $|S_{21}(\omega)|^2$ represent the reflection and transmission, respectively. The transmission coefficient is zero ($|S_{21}(\omega)|^2 \approx 0$), as a copper ground plate with a thickness of 0.035 mm is employed. So, Eq. (2) becomes

$$A(\omega) = 1 - |S_{11}(\omega)|^2 \quad (2)$$

The impedance of metamaterial is

$$z = \sqrt{\frac{\mu}{\varepsilon}} \quad (3)$$

where $\mu = \mu_o \mu_r$ and $\varepsilon = \varepsilon_o \varepsilon_r$,

The impedance of free space is

$$z_o = \sqrt{\frac{\mu_o}{\varepsilon_o}} \quad (4)$$

Fresnel formulas of reflection for TM- and TE-polarizations are

$$R_{TE} = \left(\frac{\mu_r \cos\theta - \sqrt{n^2 - \sin\theta}}{\mu_r \cos\theta + \sqrt{n^2 - \sin\theta}} \right)^2 \quad (5)$$

$$R_{TM} = \left(\frac{\varepsilon_r \cos\theta - \sqrt{n^2 - \sin\theta}}{\varepsilon_r \cos\theta + \sqrt{n^2 - \sin\theta}} \right)^2 \quad (6)$$

where μ_r and ε_r are relative permeability and permittivity. The refractive index of the metamaterial is shown by n which is equal to $\mu_r \varepsilon_r$. The incidence angle is shown by θ and for normal incident $\theta = 0^\circ$. So, the Fresnel formula becomes

$$R = \left(\frac{\sqrt{\mu}_r - \sqrt{\varepsilon}_r}{\sqrt{\mu}_r + \sqrt{\varepsilon}_r} \right)^2 = \left(\frac{z - z_o}{z + z_o} \right)^2 \quad (7)$$

As the transmission is zero due to the copper ground used in the structure,

$$A = 1 - R = 1 - \left(\frac{z - z_o}{z + z_o} \right)^2 \quad (8)$$

when the impedance of the structure matches with the free-space impedance, $z = z_o$, and unity absorption is attained.

3. RESULTS AND DISCUSSION

The evolution of the design of the metasuraface-based absorber is illustrated in Fig. 2. Firstly, absorptivity of the fine-like structure enclosed by split rings without chip resistors is depicted in Fig. 2(a). Two absorption peaks are observed at 15 and 17 GHz, respectively. It can be seen that both absorption peaks have absorptivity above 80%. Secondly, the absorption of the metasurface-based absorber composed of chip resistors is presented in Fig. 2(b). The optimized results for the absorption are attained by using 200 Ohm chip resistors. It is shown that wideband absorptivity is attained by the inclusion of the chip resistors in the design. Results show that more than 90% absorptivity is attained from 8 to 17 GHz. The structure has a four-folded symmetry; therefore, TE- and TM-polarizations have the same absorptivity which shows the structure with polarization-insensitive nature. The wideband absorption is caused by Fabry-Perot effect which is due to the

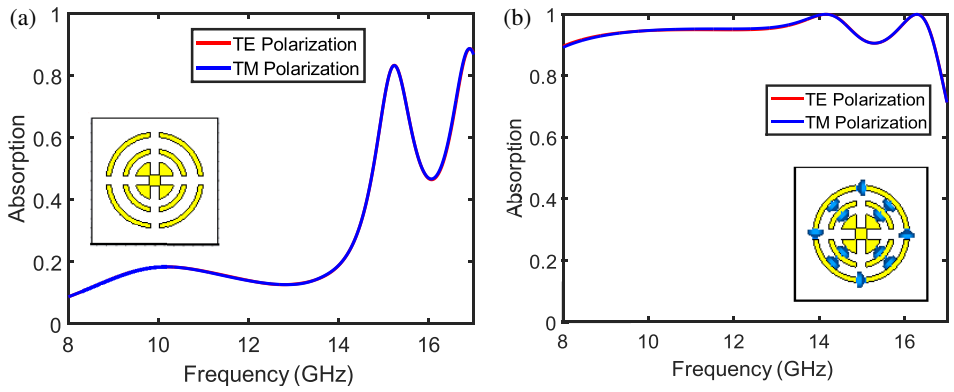

FIGURE 2. Absorptivity of the metamaterial absorber, (a) without chip resistors, (b) with chip resistors.

destructive interference that occurs between two parallel reflective surfaces. The trapped light inside the cavity undergoes multiple reflections which in turn produce the absorption. Further, the destructive interference leads to the minimal reflection, and missing energy is converted into heat.

The impedance of the media provides a clear insight of the reflection and transmission through a media. Notably, if the impedance of the media matches with the free-space wave impedance, then all incoming waves penetrate in media. The impedance of MMA is matched with the free-space impedance.

The effective impedance can be written as $Z_{eff} = \sqrt{\frac{\mu_{eff}}{\varepsilon_{eff}}}$, where ε_{eff} is the effective dielectric constant and effective permeability of the MMA.

Using S-parameters the normalized impedance can be calculated as follows [1]:

$$Z_{eff} = \sqrt{\frac{(1+S_{11})^2 - S_{21}^2}{(1-S_{11})^2 - S_{21}^2}}$$

The normalized impedance of absorber for both the real and imaginary parts is analyzed (as shown in Fig. 3). It is observed from the plot that the real part of the impedance remains 0.5 at 8 GHz, and it increases with the increase of operating frequency and reaches unity at 14 GHz. It can be observed that the incidence wave is completely absorbed at 14 GHz. For frequency

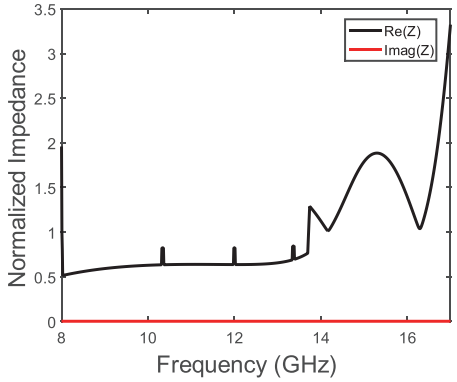

FIGURE 3. Demonstration of normalized impedance of the absorber.

17 GHz, the impedance becomes very high, and absorptivity is reduced at this value of frequency. For the entire operating frequency imaginary impedance remains zero (represented by the red line).

The surface current densities are very useful for investigating the absorption mechanism. We have considered two absorption peaks at 10 and 15 GHz to study the surface current densities (SCDs) as reported in Fig. 4. For the peak at 10 GHz, the plot for current densities is demonstrated in Figs. 4(a) and (b), respectively. On the top surface, it is observed that current is restricted on the split rings and on the wheel of the enclosed fan. The bottom layer shows the surface current in the upward direction. Currents on the top and bottom layers are antiparallel that lead to formation of magnetic dipoles. The magnetic resonance is achieved due to the magnetic dipoles. Figs. 4(c) and (d) correspond to the SCD of the top and bottom layers for 15 GHz. Similar to the previous situation, absorption is due to magnetic resonance. As clearly seen, SCDs are antiparallel for the top and bottom layers.

The effects of the angular excitation on the absorber are analyzed for TE- and TM-polarizations. The absorptivity is investigated from $\theta = 0^\circ$ to 45°. It is noticed that absorptivity remains considerably stable up to $\theta = 40^\circ$ of the excited wave; however, the trend of the reduction in the absorptivity is observed with the increase of incidence angle. For TE-polarization, the absorptivity remains above 80% from 8.5 to 16 GHz for obliquity incidence from 0° to 45° (as shown in Fig. 5(a)), whereas for TM-polarization, results show that absorptivity greatly decreases with the increase of the incidence compared with TE-polarization (as shown in Fig. 5(b)). For $\theta = 45^\circ$, a dip in the absorption is depicted at 11 GHz. Nevertheless, it remains above 80% for the remaining frequency range as obvious in Fig. 5(b) by dotted blue line. This significantly high angular stability makes the absorber useful for practical applications.

Moreover, the absorptivity is studied for varying the resistance of the chip resistor from 180 to 250 Ω for the normal incidence of the wave. Figs. 6(a) and 6(b), respectively, show the absorptivity for different values of the resistance for TE- and TM-polarizations. It is observed that absorptivity remains the same for different polarizations corresponding to their resistivity. Henceforth, it can be concluded that resistance does

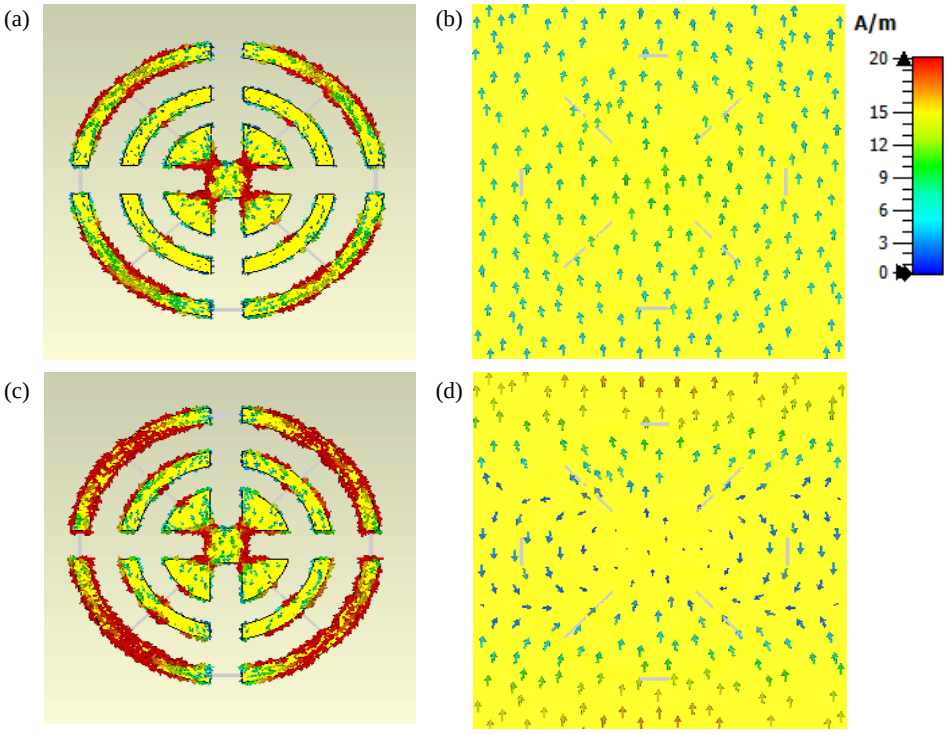

FIGURE 4. SCD, (a) top layer for 10 GHz, (b) ground layer for 10 GHz, (c) top layer for 15 GHz, (d) ground layer for 15 GHz.

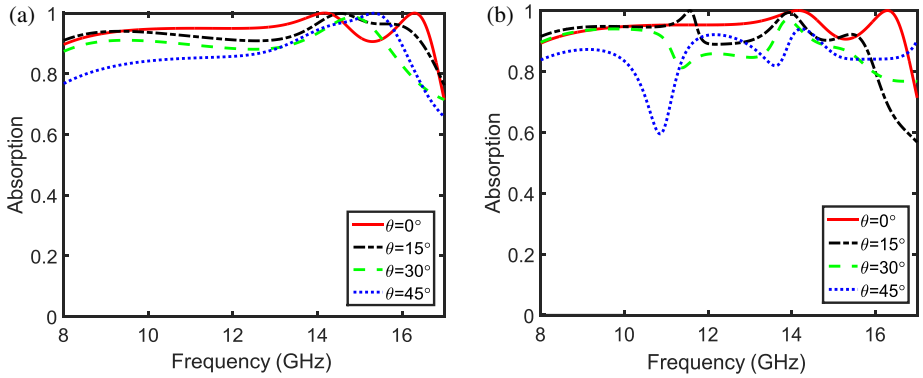

FIGURE 5. Plot for absorptivity for different values of θ, (a) for TE polarization and (b) for TM polarization.

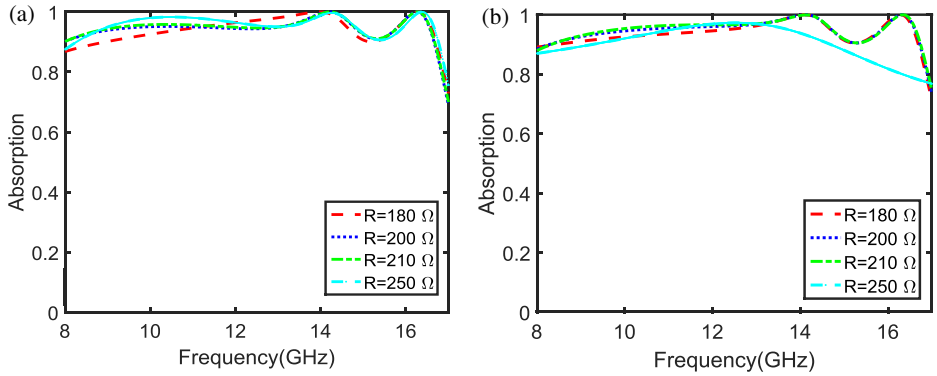

FIGURE 6. Plot for absorptivity for different values of the resistance, (a) for TE polarization and (b) for TM polarization.

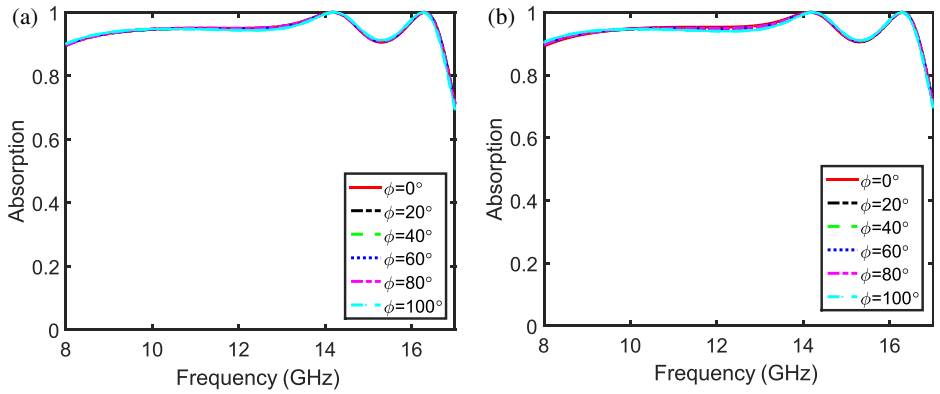

FIGURE 7. Plot for different values of φ for absorptivity, (a) for TE polarization and (b) for TM polarization.

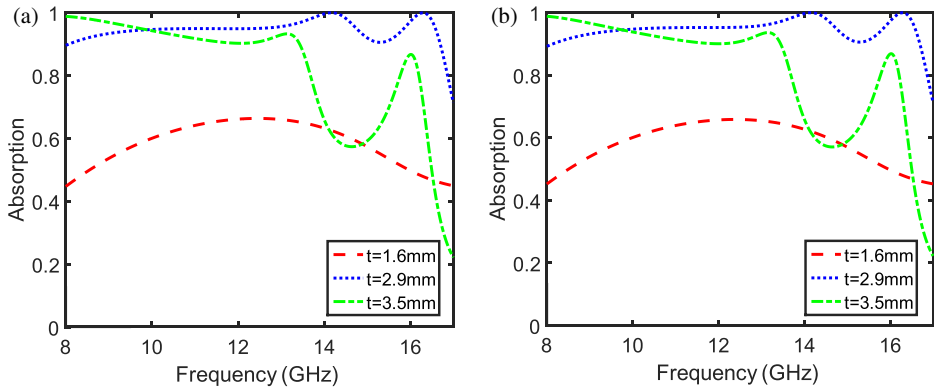

FIGURE 8. Plot for absorptivity for thickness of the substrate, (a) for TE polarization and (b) for TM polarization.

not affect polarization. It is noticed that the best results are attained at 200 Ω. In addition, the change in the resistance shows a very minor impact of the change in resistance. The absorber will remain stable despite environmental effects.

Further, consequences of the polarization φ are analyzed on the absorber keeping the chip resistor value 200 Ω (as shown in Fig. 7). Figs. 7(a) and (b), respectively, illustrate the absorptivity for the TE and TM polarizations, and it is depicted that absorptivity remains unchanged by altering the polarization for the normal incidence of the wave. This polarization-insensitivity is attained due the symmetry of the metasurface of the design.

The thickness of the substrate remains a prominent effect on the absorptivity of the absorber. The substrate traps the incoming wave from the top metasurface of the absorber and then converts it into the heat by multiple reflections of the Fabry-Perot cavity of the substrate. The plots show that absorptivity is enhanced when the absorber substrate thickness increases from 1.6 to 2.9 mm. Nonetheless, absorption bandwidth reduced as thickness increased from 2.9 to 3.5 mm. The best results are attained as the thickness is $t = 2.9$ mm (as shown Fig. 8).

Table 2 illustrates the proposed work with the reported state-of-the-art published work. Comparing the reported work, it has been noticed that the proposed absorbers have superiority in terms of absorption bandwidth, absorber configuration, and polarization-insensitive nature.

4. EXPERIMENTAL STUDY

In this section, the proposed metamaterial absorber is experimentally examined. The experimental setup is shown in Fig. 9. Before the measurements, the prototype of the proposed absorber was fabricated by the LPKF PCB prototyping machine. The prototype consists of 14×14 unit cells covering a square area of $200 \times 200\,\text{mm}^2$ with an FR4 type sample thickness of 2.9 mm. The focused view of the prototype is illustrated in Fig. 10(a). It is produced without chip resistors, and the performance is compared with a simulated one.

The absorption features of the structure are measured by two ports Agilent PNA-L vector network analyzer (VNA) having

FIGURE 9. Experimental setup for the measurement of absorption.

TABLE 2. Comparative analysis of the suggested absorber against state-of-the-art reported studies.

Reference	Operating Frequency	Material Used	Configuration	Absorption Bandwidth (> 80%)	Polarization-insensitive
[41]	8–16	FR4 and Copper	Multilayered	Multiband	Yes
[42]	1–10	FR4, Copper and Resistors	Resistive load	2–8.5	Yes
[43]	1–4.5	FR4, Copper and Resistors	Resistive load	1.9–3	Yes
[44]	2–16	FR4, Copper and Resistors Laoded Strips	Resistors laoded strips	4–12	No
[45]	2–15	FR4, Copper and Resistors		4–10	No
Present Work	8–17	FR4, Copper and Resistors	Resistive Load	8 to 16.8	Yes

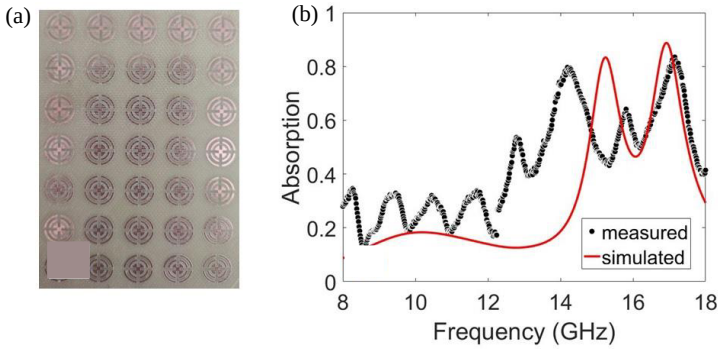

FIGURE 10. (a) Fabricated prototype and (b) numerical and experimental absorption performances for the metamaterial absorber without chip resistors.

an operating frequency band between 10 MHz and 43.5 GHz. Before the measurements, one of the ports of the VNA was calibrated by way of unguided calibration settings including load, short and open circuit techniques. During the measurements, a horn antenna between the frequencies of 3 GHz and 18 GHz is used to observe the S_{11} result. There is a linear relationship between the far-field region and frequency, which can be calculated as follows.

$$Farfield = \frac{2D^2}{\lambda} \tag{9}$$

where D (8 mm) is the maximum antenna aperture, and λ (28.5 mm) represents the wavelength of the central frequency. Using this formula, the starting point of the far-field region is found to be 445 mm. Therefore, meticulous attention was given to maintaining a separation between the prototype and the horn antenna that exceeds this threshold.

The measured and simulated absorption results of the proposed metamaterial absorber without chip resistors are demonstrated in Fig. 10(b). In numerical studies, the maximum absorption peaks are obtained at frequencies of 15.75 GHz and 16.88 GHz. At these peaks, the absorption ratios are monitored above 80%. In the experimental studies, similar peaks with almost the same absorption ratios are obtained at the frequencies of 14.16 GHz and 17.08 GHz. When the simulation and measurement results are compared to each other, a frequency shift can be observed, especially at the first absorption peak in the plot. Despite this exact unmatched condition, the absorption ratios of both results are almost at the same level. Therefore, the experimental study gives thought to the performance of the proposed absorption. The sources of the distortions and frequency shift in the measurement result stem from various conditions. As can be seen in Fig. 9, the experimental study could not be realized by using an anechoic chamber. Besides, the -3 dB beamwidth of the antenna should be larger than the sample size to ensure uniform illumination. Horn antennas can be characterized by their beamwidth which can be stated as

$$\theta \approx \frac{\lambda}{D} \tag{10}$$

It results in a relatively narrow beamwidth of approximately 20.4 degrees. Due to this relatively narrow beamwidth, the absence of an anechoic chamber and alignment of the sample may cause some discrepancies between simulations and experiments. In addition to the experimental environmental conditions, the fabrication errors which especially occur during carving around the unit cell by a lack of sensitivity cause the resonance frequency shift. Despite these limitations, it can be concluded that the simulated results in Fig. 10 align well with the experimental one and offer valuable insights.

5. CONCLUSION

The study examines a broadband metamaterial absorber composed of chip resistors, as detailed in the preceding results and discussion. The incorporation of chip resistors in the design has significantly enhanced the absorption capacity. It is observed that above 80% of radar signals get absorbed with an absorption bandwidth of 8.9 GHz, including the X- and Ku-bands. In addition, the absorber shows polarization insensitivity and wide-angle absorptivity which make this absorber useful for industrial applications. The simulation results are compared with the measured ones. It is noticed that the measured and simulated results show an agreement.

ACKNOWLEDGEMENT

M. A. Baqir, A. Qadeer, O and U. Draz gratefully acknowledge the support of the Higher Education Commission, Pakistan (20-491 14992/NRPU/R\D/HEC/2021 2021).

Jahariah Sampe would like to acknowledge work is funded by the Ministry of Higher Education (MOHE), Malaysia under Fundamental Research Grant Scheme (FRGS) with code FRGS/1/2024/TK07/UKM/02/9.

REFERENCES

[1] Smith, D. R., W. J. Padilla, D. C. Vier, S. C. Nemat-Nasser, and S. Schultz, "Composite medium with simultaneously negative permeability and permittivity," *Physical Review Letters*, Vol. 84, No. 18, 4184, 2000.

[2] Lemoult, F., N. Kaina, M. Fink, and G. Lerosey, "Wave propagation control at the deep subwavelength scale in metamaterials," *Nature Physics*, Vol. 9, No. 1, 55–60, 2013.

[3] Kadic, M., T. Bückmann, R. Schittny, and M. Wegener, "Metamaterials beyond electromagnetism," *Reports on Progress in Physics*, Vol. 76, No. 12, 126501, 2013.

[4] Kaina, N., F. Lemoult, M. Fink, and G. Lerosey, "Negative refractive index and acoustic superlens from multiple scattering in single negative metamaterials," *Nature*, Vol. 525, No. 7567, 77–81, 2015.

[5] Zheludev, N. I., "The road ahead for metamaterials," *Science*, Vol. 328, No. 5978, 582–583, 2010.

[6] Liu, Y. and X. Zhang, "Metamaterials: A new frontier of science and technology," *Chemical Society Reviews*, Vol. 40, No. 5, 2494–2507, 2011.

[7] Tsai, K.-T., G. A. Wurtz, J.-Y. Chu, T.-Y. Cheng, H.-H. Wang, A. V. Krasavin, J.-H. He, B. M. Wells, V. A. Podolskiy, J.-K. Wang, Y.-L. Wang, and A. V. Zayats, "Looking into meta-atoms of plasmonic nanowire metamaterial," *Nano Letters*, Vol. 14, No. 9, 4971–4976, 2014.

[8] Pendry, J. B., "Negative refraction makes a perfect lens," *Physical Review Letters*, Vol. 85, No. 18, 3966, 2000.

[9] Sato, Y., K. Izui, T. Yamada, and S. Nishiwaki, "Robust topology optimization of optical cloaks under uncertainties in wave number and angle of incident wave," *International Journal For Numerical Methods in Engineering*, Vol. 121, No. 17, 3926–3954, 2020.

[10] Liu, B., H. Giddens, Y. Li, Y. He, S.-W. Wong, and Y. Hao, "Design and experimental demonstration of Doppler cloak from spatiotemporally modulated metamaterials based on rotational Doppler effect," *Optics Express*, Vol. 28, No. 3, 3745–3755, 2020.

[11] Neubrech, F., M. Hentschel, and N. Liu, "Reconfigurable plasmonic chirality: Fundamentals and applications," *Advanced Materials*, Vol. 32, No. 41, 1905640, 2020.

[12] Ghasemi, M., M. A. Baqir, and P. K. Choudhury, "On the metasurface-based comb filters," *IEEE Photonics Technology Letters*, Vol. 28, No. 10, 1100–1103, 2016.

[13] Baqir, M. A. and P. K. Choudhury, "Toward filtering aspects of silver nanowire-based hyperbolic metamaterial," *Plasmonics*, Vol. 13, 2015–2020, 2018.

[14] Baqir, M. A., P. K. Choudhury, A. Farmani, T. Younas, J. Arshad, A. Mir, and S. Karimi, "Tunable plasmon induced transparency in graphene and hyperbolic metamaterial-based structure," *IEEE Photonics Journal*, Vol. 11, No. 4, 4601510, Aug. 2019.

[15] Baqir, M. A. and P. K. Choudhury, "On the VO2 metasurface-based temperature sensor," *Journal of the Optical Society of America B*, Vol. 36, No. 8, F123–F130, 2019.

[16] Hoque, A. K. M. H., M. Z. Islam, M. A. Sakib, and Y. Tsui, "Using high-k VPP modes in grating-coupled graphene-based hyperbolic metamaterial for tunable sensor design," *IEEE Sensors Journal*, Vol. 21, No. 16, 17 790–17 799, Aug. 2021.

[17] Zou, H. and Y. Cheng, "Design of a six-band terahertz metamaterial absorber for temperature sensing application," *Optical Materials*, Vol. 88, 674–679, Feb. 2019.

[18] Qin, F., X. Chen, Z. Yi, W. Yao, H. Yang, Y. Tang, Y. Yi, H. Li, and Y. Yi, "Ultra-broadband and wide-angle perfect solar absorber based on TiN nanodisk and Ti thin film structure," *Solar Energy Materials and Solar Cells*, Vol. 211, 110535, Jul. 2020.

[19] Liu, H., M. Xie, Q. Ai, and Z. Yu, "Ultra-broadband selective absorber for near-perfect harvesting of solar energy," *Journal of Quantitative Spectroscopy and Radiative Transfer*, Vol. 266, 107575, 2021.

[20] Cheng, Y., R. Xing, F. Chen, H. Luo, A. A. Fathnan, and H. Wakatsuchi, "Terahertz pseudo-waveform-selective metasurface absorber based on a square-patch structure loaded with linear circuit components," *Advanced Photonics Research*, Vol. 5, No. 8, 2300303, 2024.

[21] Baqir, M. A. and P. K. Choudhury, "Hyperbolic metamaterial-based UV absorber," *IEEE Photonics Technology Letters*, Vol. 29, No. 18, 1548–1551, 2017.

[22] Qian, Y., Y. Cheng, H. Luo, F. Chen, A. A. Fathnan, and H. Wakatsuchi, "Design of a dual-band waveform-selective metasurface absorber based on the combination of two resonator structures loaded with nonlinear circuits," *Advanced Theory and Simulations*, Vol. 7, No. 4, 2300590, 2024.

[23] Bilal, R. M. H., M. A. Baqir, P. K. Choudhury, M. M. Ali, and A. A. Rahim, "Tunable and multiple plasmon-induced transparency in a metasurface comprised of silver s-shaped resonator and rectangular strip," *IEEE Photonics Journal*, Vol. 12, No. 3, 4500913, 2020.

[24] Bilal, R. M. H., M. A. Baqir, M. Hameed, S. A. Naqvi, and M. M. Ali, "Triangular metallic ring-shaped broadband polarization-insensitive and wide-angle metamaterial absorber for the visible regime," *Journal of the Optical Society of America A*, Vol. 39, No. 1, 136–142, 2022.

[25] Baqir, M. A., H. Latif, O. Altintas, M. N. Akhtar, M. Karaaslan, H. Server, M. Hameed, and N. M. Idrees, "Fractal metamaterial based multiband absorber operating in 5G regime," *Optik*, Vol. 266, 169626, 2022.

[26] Cai, B., L. Yang, L. Wu, Y. Cheng, and X. Li, "Dual-narrowband terahertz metamaterial absorber based on all-metal vertical ring array for enhanced sensing application," *Physica Scripta*, Vol. 99, No. 9, 095503, 2024.

[27] Wang, Z., Y. Wan, H. Luo, S. Lv, S. Yan, Y. Cheng, F. Chen, and X. Li, "Deep learning-assisted design optically transparent metamaterial absorber with infrared-microwave compatible camouflage," *Applied Materials Today*, Vol. 42, 102588, 2025.

[28] Landy, N. I., S. Sajuyigbe, J. J. Mock, D. R. Smith, and W. J. Padilla, "Perfect metamaterial absorber," *Physical Review Letters*, Vol. 100, No. 20, 207402, 2008.

[29] Ozden, K., O. M. Yucedag, and H. Kocer, "Metamaterial based broadband RF absorber at X-band," *AEU — International Journal of Electronics and Communications*, Vol. 70, No. 8, 1062–1070, 2016.

[30] Shi, M., C. Xu, Z. Yang, J. Liang, L. Wang, S. Tan, and G. Xu, "Achieving good infrared-radar compatible stealth property on metamaterial-based absorber by controlling the floating rate of Al type infrared coating," *Journal of Alloys and Compounds*, Vol. 764, 314–322, 2018.

[31] Ozden, K., O. M. Yucedag, and H. Kocer, "Metamaterial based broadband RF absorber at X-band," *AEU — International Journal of Electronics and Communications*, Vol. 70, No. 8, 1062–1070, 2016.

[32] Siva Nagasree, P., K. Ramji, M. K. Naidu, and T. C. Shami, "X-band radar-absorbing structures based on MWCNTs/NiZn ferrite nanocomposites," *Plastics, Rubber and Composites*, Vol. 50, No. 2, 71–82, 2021.

[33] Rani, M., K. S. Bhatia, H. Singh, H. Kaur, and N. Gupta, "Synthesis of suitable material for microwave absorbing properties in X-band," *SN Applied Sciences*, Vol. 2, No. 12, 2035, 2020.

[34] Teng, D., Y. Yang, J. Guo, W. Ma, Y. Tang, and K. Wang, "Efficient guiding mid-infrared waves with graphene-coated nanowire based plasmon waveguides," *Results in Physics*, Vol. 17, 103169, 2020.

[35] Lai, Y.-C., C.-Y. Chen, Y.-T. Hung, and C.-Y. Chen, "Extending absorption edge through the hybrid resonator-based absorber with wideband and near-perfect absorption in visible region," *Materials*, Vol. 13, No. 6, 1470, 2020.

[36] Hoa, N. T. Q., P. H. Lam, P. D. Tung, T. S. Tuan, and H. Nguyen, "Numerical study of a wide-angle and polarization-insensitive ultrabroadband metamaterial absorber in visible and near-infrared region," *IEEE Photonics Journal*, Vol. 11, No. 1, 1–8, 2019.

[37] Bao, L. and T. J. Cui, "Tunable, reconfigurable, and programmable metamaterials," *Microwave and Optical Technology Letters*, Vol. 62, No. 1, 9–32, 2020.

[38] Hao, J., B. Zhang, H. Jing, Y. Wei, J. Wang, Z. Qu, and J. Duan, "A transparent ultra-broadband microwave absorber based on flexible multilayer structure," *Optical Materials*, Vol. 128, 112173, 2022.

[39] Wei, J., Y. He, S. Bie, S. Wu, Z. Lei, W. Deng, Y. Liu, Y. Zhang, C. Li, J. Ai, and J. Jiang, "Flexible design and realization of wideband microwave absorber with double-layered resistor loaded FSS," *Journal of Physics D: Applied Physics*, Vol. 52, No. 18, 185101, 2019.

[40] Yin, X., C. Long, J. Li, H. Zhu, L. Chen, J. Guan, and X. Li, "Ultra-wideband microwave absorber by connecting multiple absorption bands of two different-sized hyperbolic metamaterial waveguide arrays," *Scientific Reports*, Vol. 5, No. 1, 15367, 2015.

[41] Wen, D.-e., X. Huang, L. Guo, H. Yang, S. Han, and J. Zhang, "Quadruple-band polarization-insensitive wide-angle metamaterial absorber based on multi-layer structure," *Optik*, Vol. 126, No. 9-10, 1018–1020, May 2015.

[42] Peng, J., C. Li, F. Cheng, L. Wu, W.-W. Xu, and Z.-J. Liu, "Resistor-loaded wideband polarization independent absorber using tightly coupled dipole structure," *International Journal of RF and Microwave Computer-Aided Engineering*, Vol. 2024, No. 1, 5321173, 2024.

[43] Amer, A. A. G., S. Z. Sapuan, N. B. Othman, A. A. Salem, A. J. A. Al-Gburi, and Z. Zakaria, "A wide-angle, polarization-insensitive, wideband metamaterial absorber with lumped resistor loading for ISM band applications," *IEEE Access*, Vol. 12, 42 629–42 641, 2023.

[44] Zhang, M., B. Zhang, X. Liu, S. Sun, and C. Jin, "Design of wideband absorber based on dual-resistor-loaded metallic strips," *International Journal of Antennas and Propagation*, Vol. 2020, No. 1, 1238656, 2020.

[45] Lin, X. Q., P. Mei, P. C. Zhang, Z. Z. D. Chen, and Y. Fan, "Development of a resistor-loaded ultrawideband absorber with antenna reciprocity," *IEEE Transactions on Antennas and Propagation*, Vol. 64, No. 11, 4910–4913, 2016.